Infrared thermography applied to the validation of thermal simulation of high luminance LED used in automotive front lighting

By C. Rongier*,**, R. Gilblas*, Y. Le Maoult*, S. Belkessam**, F. Schmidt*

* Université de Toulouse, IMT Mines Albi (Institut Clément Ader), Campus Jarlard, F-81013, Albi cedex 09 France
** Valeo Lighting System, 34 rue Saint André, 93102 Bobigny, France

Highlights

- The thermal behavior of a high luminance LED emitting a luminous energy of 3000lm and dissipating a thermal power of 40W is investigated.
- A numerical thermal model of the LED is developed based on Finite Volume Flow Simulation (FVM). The inputs of the model have been characterized by Scanning Electron Microscopy (SEM), T3ster method, goniometry and Fourier transform infrared (FITR) spectrometry.
- Adapted metrology has been developed to address a challenging thermography temperature measurement method: due to the small-dimensions and multi-materials nature of the LED stack-up, a specific test bench has then been designed for measuring LED temperature.
- Finally, comparison of IR thermography results versus 3D thermal simulation are achieved with a deviation lower than 5%, and emphasizes the good agreement between simulations and experiments.

Abstract

Automotive front lighting evolved toward digital and adaptive high definition beams. In order to create such functions, multiple LED designs are replaced with new LED concepts involving only one high luminance LED. The luminous energy emitted by such a semiconductor light source, up to 3000lm (*i.e.* 10W), induces high density of energy up to 40W that requires to be thermally managed. Indeed, optical performances and reliability of components are directly linked to the LED temperature. Thus, accurate and efficient numerical models must be developed. In this paper, the validation of the high luminance LED thermal model is achieved by comparing numerical simulations with experimental data. The full characterization of the components is managed in order to build the corresponding thermal model. Then, a well-designed experimental set-up was developed to proceed to LED temperature measurement thanks to IR thermography, involving a camera equipped with a macro lens G1. A temperature uncertainty calculation is performed to introduce a tolerance range for the validation of the software. Finally, the commercial FVM software FloEFD™ is used to compute the LED thermal model. Numerical simulations are compared to experimental data. The agreement between computations and IR thermography is fair, which reinforces the use of the developed model with acceptable accuracy.

Keywords

High luminance LED, Infrared thermography, Thermo-optical properties characterization, calibration, Spectrometry, 3D thermal simulation.

1. Introduction

Automotive lighting technologies experience an important growth in terms of lighting functionalities such as glare free beams [1]. According to this trend, LED designs are replaced by new LED sources that provide high definition beams [2]. The non-homogeneous luminous flux emitted by these optoelectronic components induce a high density of energy that requires to be thermally managed. Indeed, the thermal management of high power LED system is of prime interest to ensure both optical performances and components reliability [3] [4]. The thermal behavior of the semiconductor light source allows determining the junction temperature of the components. Several ways exist to estimate LED junction temperature. Method based on thermal transient heat transfer measurement, exploiting the cumulative structure function of the LED, allows determining the thermal resistance. This quantity is then implemented in models in order to estimate the junction temperature [5] [6]. The thermal transient heat transfer measurement, also known as the forward voltage for LED analysis, is sensitive to current and/or voltage instability for new LED chips [7]. Moreover, this approach cannot provide information regarding the spatial distribution of LED temperature. Therefore, it cannot been applied if temperature gradients occurs in the LED chips.

An alternative model-free method is the direct measurement of LED temperature by IR thermography [8] [9]. This approach is convenient to visualize the heat spreading through a LED system [10]. However, the quantitative measurement of LED temperature can be very complex and can lead to inaccurate results. First, the stack-up structure of the LED as well as the visible, local emission of energy induce significant deviation between LED junction and surface temperature [11]. Moreover, the emissivity of the surface needs to be well known to proceed to quantitative IR thermography. To face this issue, several researchers have considered assumptions and/or the value of emissivity is set according to reference tables [12]. Other approaches consist in depositing a high emissive thin-film coating on the LED surface [13] [14]. This modify the radiative properties of the LED emitting area, and can affect the thermal behavior of the light source To overcome this problem, a temperature measurement must be performed with a thermocouple and the emissivity setting of the IR unit must be adjusted to match these results [10]. However, this method is not adapted for measuring LED temperature since the light absorption induce the thermocouple self-heating. This leads to an error on the emissivity value, and consequently on the apparent temperature measured by the infrared device [15]. The knowledge of the LED emissivity is so a real problem for carrying out a temperature measurement involving IR thermography. Moreover, the LED architecture is based on a stack-up structure. It is so essential to characterize the radiative properties of each layer, since the semi-transparent nature of the semi-conductor materials influences the results of thermal infrared imaging substantially [16]. Then, the small dimensions of the LED can affect the IR thermography measurement, since the spatial resolution is still a limiting factor [17] [18]. Thus, a high spatial resolution is required to capture the temperature distribution of a LED.

In this paper, an original technique for the quantitative measurement of the temperature of a high luminance LED (which dissipated power is greater than 40W) is proposed. **Fig. 1** illustrates the semiconductor light source architecture.

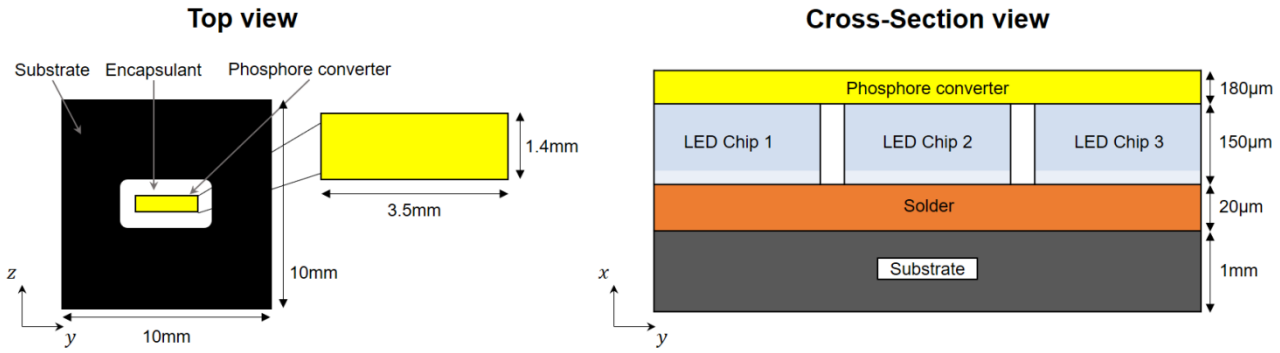


Fig. 1 – Sketch of the LED structure

In the proposed technique, IR thermography involving a camera equipped with a macro lens G1 is used to measure quantitatively the LED temperature and then to proceed to thermal simulation model validation. To build the LED thermal model, the whole components characterization has been performed, in terms of structural analysis, optical performances and thermal behavior. The emissivity characterization of LED was challenging due to the semi-transparent, multi-layers and small size nature of the light source. A specific method using IRTF spectrometry methodology has then been developed. The calibration of the IR device, as well as the uncertainties budget, have been performed to determine the measurement uncertainty. Finally, results obtained from IR thermography are compared with numerical results to proceed to high luminance LED 3D thermal model validation. The paper is organized as follows. In section 2, the semiconductor light source structure is characterized, and the thermal, optical and radiative properties of the LED are measured. From this characterization, the 3D thermal model of the semiconductor light source is developed. In section 3, thanks to the characterization of the LED active region emissivity, a choice in terms of the most adapted IR device is made for proceeding to LED temperature measurement. The calibration steps as well as the measurement accuracy are investigated. Finally, LED temperature measurement under different operating conditions are carried out in section 4, and the results leads to the validation of the 3D thermal simulation of the LED.

2. Presentation of the components and characterization

This section describes the characterization of the high luminance LED, to supply the numerical model developed in next section. SEM analysis and structure function characterization are performed in order to accurately know the internal architecture of the component. Then, the LED optical performances are characterized by photometry in order to estimate the dissipated power used as boundary conditions in the thermal simulation set up. Finally, infrared spectrometry is performed on LED active region in order to determine its emissivity and then proceed to temperature measurement by IR thermography.

2.1. SEM analysis

The cross-section observation of the high luminance LED sample by scanning electron microscopy (SEM) is shown in **Fig. 2**. Regarding the electrical insulating nature of the material, the low vacuum mode was used and the Gaseous Analytical Detector (GAD) with an acceleration voltage of 20kV enables a chemical contrast on the sample and the separation of each layer. SEM observations show the structure consists of a stack-up involving several material layers (from the top to the bottom). The phosphor converter layer consists of a YAG:Ce^{3+} doped ceramic glass as developed in [19]. Such

a system is suited as a conversion layer involved in white LED. The composition of this layer highlights that the Ce:YAG concentration is low in the glass matrix (up to 5%wt according to [20]). Then, a silicone substrate allows the deposition of the phosphor converter on the blue LED chips (layer of 147µm thickness). Since the LED is based on a flip-chip architecture, as described in [21], the active region consisting of N and P-type GaN semiconductors is deposited on a sapphire substrate and is then inverted. Finally, LED chips are bonded on a ceramic substrate with a specific interface that contains bumps. Due to the confidentiality of such a component, it is not possible to provide further information regarding the composition of the material.

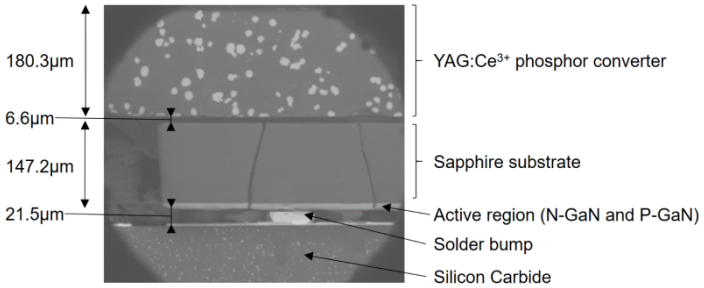


Fig. 2 – SEM analysis of high luminance LED structure

2.2. LED structure function and thermal resistance

The determination of the LED thermal resistance requires to perform Transient Dual Interface measurement [22]. This experimental method is used to measure the thermal impedance of the component, and to convert it into cumulative structure functions. The impedance measurement is carried out by the Thermal Transient Tester (T3ster) [23]. As illustrated on **Fig. 3**, this system is composed with:

- A power supply ;
- A LED control unit and a thermal characterization system, the so called T3ster ;
- A radiometric characterization device, equipped with an integrating sphere.

The radiometric characterization device measures the optical power emitted by the component. Its transient thermal behavior is then characterized by applying the energy balance governing the functioning of the LED.

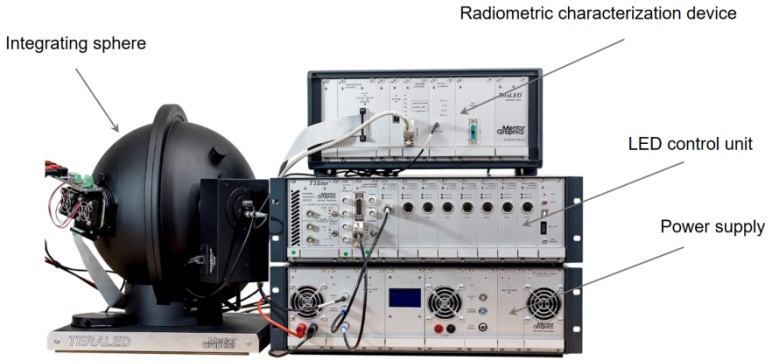


Fig. 3 – Thermal Transient Tester (T3ster)

Based on R-C network, it allows obtaining the cumulative structure function of the component, which represents dependence of the cumulative thermal capacitance on cumulative thermal resistance values along the main heat path of the LED during test [24] (see **Fig. 4**). The measurement is performed by considering the same LED and cold plate but different thermal interfaces. First, the LED is positioned on the cold plate with an interface ①. After characterization, the blue curve on the figure is obtained and corresponds to the cumulative structure function of the system {LED + interface ① + cold plate}. In order to determine the thermal resistance of LED, a second measurement has been performed, with a better thermal interface called interface ② (red curve). Since, the LED is the same in each configuration, the cumulative structure function of the component is the same. However, when the heat flux reaches the thermal interface, a separation point occurs since the thermal resistance of both interface are different. Finally, the separation point of the two cumulative structure functions allows determining the LED thermal resistance that is equal to 0.85K/W. This data is crucial for understanding the thermal behavior of the component and is essential for validating the thermal model.

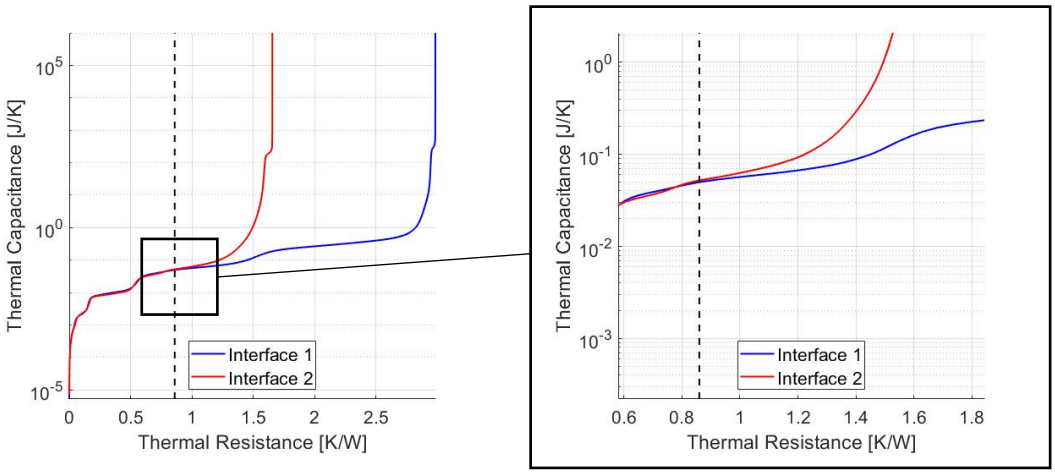


Fig. 4 – Cumulative structure function of high luminance LED

2.3. LED optical performances

In order to determine the dissipated power of the LED, electrical power consumed by the LED and optical power emitted by the LED are required. The electrical power is determined by measuring both current intensity and forward voltage while the LED is operating. However, for characterizing the optical performances of the LED mounted on its cooling system, a specific experiment has been performed and is described below. First, the radiation pattern of the LED is characterized and compared to a Lambertian emission. Then and based on the emission behavior, the luminous flux and the optical power emitted by the light source are characterized.

The spectral radiant flux emitted by the source is measured thanks to a goniometer which detector is a Si photodiode that diameter is 30mm and located at a distance of 2.5m from the goniometer. The goniometer allows scanning the angle of emission over all the hemisphere location. The angular distribution of the LED is plotted using polar coordinates, as shown in **Fig. 5**. It can be seen that, for an angle between 0° and 50°, the relative deviation between the real emission and the Lambertian one is less than 2%. However, when the angle reaches the value of 80°, the deviation reaches a value of 80%. Since irradiance for grazing angles is low, the signal on noise ratio for such conditions is poor and explains the deviation. Furthermore, the normalized irradiance obtained for 80° is lower

than 0.1, which means the emitted energy can be neglected. Therefore, the LED optical behavior can be assumed Lambertian.

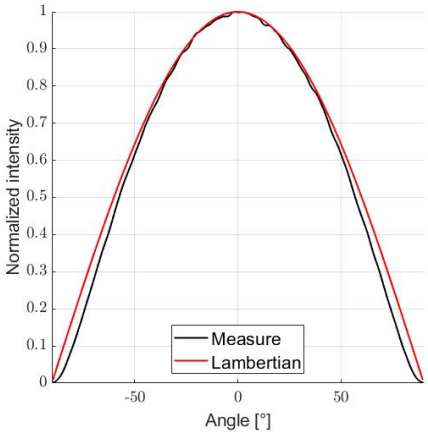


Fig. 5 – Comparison of LED radiation pattern with Lambertian emission

The luminous flux is required to proceed to energy balance of the LED. The use of an integrating sphere was not possible here since the LED is mounted on its cooling system. For that reason, the luminous flux is computed by integrating the spectral radiant flux over the angular directions (with an angular symmetry assumption) and over LED spectral range [25], as shown in **Fig. 6**.

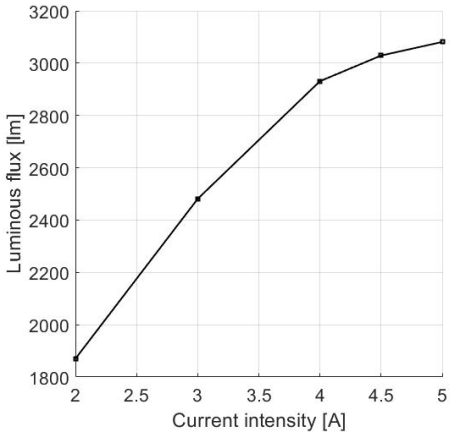


Fig. 6 – Evolution of the luminous flux versus current intensity

As expected, the luminous flux increases with the LED current intensity until reaching a maximum value. When the current intensity is too high, a large amount of energy is dissipated. Hence, the dissipated heat is partially evacuated towards the cooling system that induces an increase of LED temperature and consequently a loss of luminous flux. Here the asymptote is not reached to avoid the LED degradation but the evolution of the flux is clearly bending. As seen above, the light source is compose with three LED chips. To determine the luminous flux, emitted per chips, luminance measurement have performed similarly to [26]. Regarding this experiment, a LMK 5 camera equipped with a CCD sensor (resolution of 1380x1030 pixels) has been involved. Knowing the luminance emitted per chip and since the LED has the same behavior as a Lambertian source (see **Fig. 5**), the luminous flux emitted per chips is determined as follow:

$$\Phi_{opt} = \pi L S \quad \#\text{Eq. (1)}$$

where Φ_{opt} is the luminous flux, S the surface radiating in accordance with Lambert's law with a luminance L [25]. Knowing the luminous flux emitted per LED chips, it is now possible to determine the emitted optical power and consequently to determine the corresponding thermal power.

The LED spectrum has been characterized with a spectrometer LABSPHERE CDS 610 in the spectral range [300nm – 1000nm], as shown in **Fig. 7**. It can be seen that two peaks are obtained respectively at the wavelength of 450nm and 555nm. The first peak correspond to the energy emitted by the blue LED chips. The second peak (extended in the bandwidth [500-700]nm) corresponds to the absorption of blue energy within the phosphor converter and re-emission of yellow energy that generates, *in fine*, the white light.

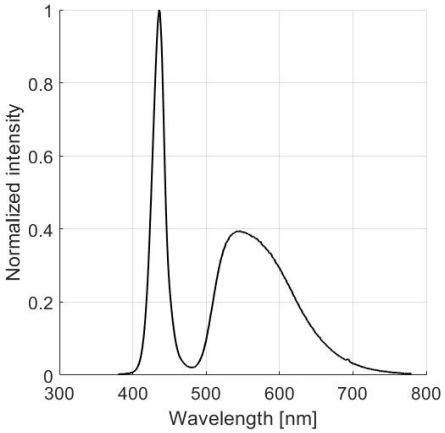


Fig. 7 – High luminance LED emission spectrum

Once the luminous flux as well as the LED spectrum are characterized, the luminous efficiency (in [lm/W]) of the LED is computed using Eq. (2).

$$K = \frac{K_m \int_0^\infty \Phi_{e,\lambda}(\lambda) V(\lambda) d\lambda}{\int_0^\infty \Phi_{e,\lambda}(\lambda) d\lambda} \#\text{Eq. (2)}$$

where $K_m = 683 lm/W$ is the photopic luminous efficiency at a wavelength of 555nm, $\Phi_{e,\lambda}(\lambda)$ is the spectral radiant flux and $V(\lambda)$ is the photopic luminosity function that describes the average spectral sensitivity of the human visual perception of brightness [27].

The calculation of the LED luminous efficiency gives a value of 314lm/W. Knowing the luminous flux Φ_{opt} [lm], the optical power P_{opt} [W] emitted by the LED is calculated as follows:

$$P_{opt} = \frac{\Phi_{opt}}{K} \#\text{Eq. (3)}$$

Results of the previous quantities are regrouped in **Tab. 1**. One can notice that the luminous energy emitted by the left chip is 16% higher than the other are. Thus, the thermal dissipation occurring in the left chip is higher than other chip as well.

Location	Chip left	Chip center	Chip Right
Luminous flux	1130 lm	974 lm	971 lm
Optical power	3.6W	3.1W	3.1W
Thermal power	16.2W	13.7W	13.7W

Tab. 1 – Luminance measurement per chips on the high luminance LED for I=5A

2.4. Energy balance

Based on the knowledge of electrical power and emitted flux, it is possible to determine the dissipated power that is applied as boundary conditions in the simulation process. **Fig. 8** describes the energy balance occurring while LED is operating.

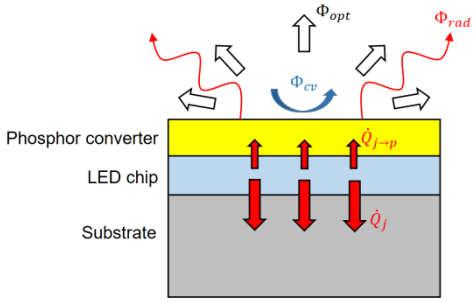


Fig. 8 – Energy balance applied on LED components

The energy balance results in the following equation.

$$P_{elec} = P_{opt} + P_{th} \#\text{Eq. (4)}$$

where P_{elec}, P_{opt} and P_{th} represent respectively the electrical power, the optical power and the thermal power dissipated by the source. **Tab. 2** regroups the total energy balance for two configurations (2A and 5A).

Current intensity [A]	Forward voltage [V]	Luminous flux [lm]	Electrical power [W]	Optical power [W]	Thermal power [W]
2	9.6	1850	19.2	5.9	13.3
5	10.7	3080	53.5	9.8	43.7

Tab. 2 – Energy balance of the high luminance LED in each configuration

The thermal power dissipated by the source can be split in four terms, as shown in Eq. (5) :

$$P_{th} = \dot{Q}_j + \dot{Q}_{j\to p} + \Phi_{rad} + \Phi_{cv} \#\text{Eq. (5)}$$

where $\dot{Q}_j$ is the dissipated power at the junction location, $\dot{Q}_{j\to p}$ is the dissipated power occurring during the blue-white conversion process, Φ_{rad} is the radiative heat flux emitted by the LED at the phosphor converter temperature and Φ_{cv} is the convective heat flux between the phosphor converter surface and the ambient environment, as detailed in [28]. **Tab. 3** proposes the evaluation of each terms in Eq. (5). For that, the radiative heat flux Φ_{rad} is estimated based on a blackbody assumption (for a temperature of 140°C). Regarding the convective heat flux Φ_{cv}, the exchange coefficient h is calculated using a correlation based on free convection on a vertical surface [29].

Total heat flux	Radiative heat flux	Convective heat flux
	T_w= 140°C – T_∞=25°C	T_w= 140°C – T_∞=25°C
	L = 1cm – S = 1cm²	L = 1cm – S = 1cm²
	$\varepsilon = 1$ (assumed as blackbody)	Rayleigh number : Ra = 8058 Nusselt number: $\mathrm{Nu}=0.825+\frac{0.387(Ra)^{1/6}}{\left[1+\left(\frac{0.49}{Pr}\right)^{9/16}\right]^{8/27}}=2.27$ Exchange coefficient: h=6.8W/m²K
P_{th}= 40W	$\Phi_{rad} = \sigma S(T_w^4 - T_\infty^4) =$ 0.12W	$\Phi_{cv} = hS(T_w - T_\infty) =$ 0.078W

Tab. 3 – Evaluation of heat transfer contribution applied to a high luminance LED

According to previous estimation, one can notice that both radiative and convective heat flux are not preponderant. Nevertheless, the radiative heat flux will be used for measuring LED temperature thanks to infrared thermography. For that, the emissivity of the LED active region is required.

2.5. Characterization of LED emissivity

The emissivity characterization on this LED is challenging for two main reasons: the size of the components (a few mm) and its multi-layer semi-transparent nature. Literature is poor about the radiative properties in the infrared spectral band of such a component. Classical integrating sphere IRTF reflectivity measurement cannot be applied without supplementary justifications and modifications.

About the semi-transparency, the study of optical properties will be conducted layer by layer. First, on the top surface of the LED is the phosphor converter. In a previous study, Xia *et al.* [30] have focused on YAG:Ce^{3+} phosphor properties: for sintering temperature between 800°C and 1000°C, phosphor transmission spectrum has been characterized with FTIR spectrometry. In the spectral band [2.5 – 5]µm, when the sintering temperature increases, the YAG:Ce^{3+} phosphor transmission increases as well, until reaching the constant value of 90% (for a sintering temperature of 1000°C). This means that the YAG:Ce3+ is transparent in this spectral region.

As discussed above, the concentration of Ce:YAG in the ceramic glass matrix is about 5%. Hence, the optical properties of the phosphor converter are mainly governed by the matrix itself. It is critical to determine if the ceramic glass is either opaque or semi-transparent in the infrared region. A simple observation of the LED thanks to an infrared camera FLIR SC7000 operating in the BII band (between 2.5 to 5µm) and equipped with a macroscopic lens Orion G1 reveals the three active junctions located in the depth of the LED (see **Fig. 9**).

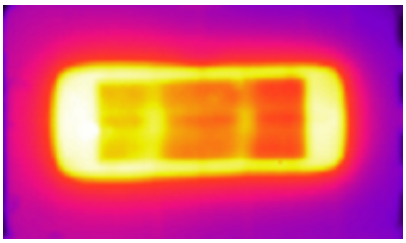


Fig. 9 – IR capture of the LED by a camera FLIR SC7000 and a G1 lens

This result shows that the monobloc layer on the top of the LED (phosphor converter) is semi-transparent and not much scattering. Moreover, and as explained in paragraph 2.1, the LED structure is based on a flip-chip architecture, in which sapphire substrate is involved. **Fig. 10** proposes the visualization of the sapphire transmission in the spectral band [2 – 10]µm, obtained for a thickness of 0.53mm. It can be seen that the sapphire is transparent in the spectral range [2.5 – 5.5]µm and the cut-off wavelength of around 7µm.

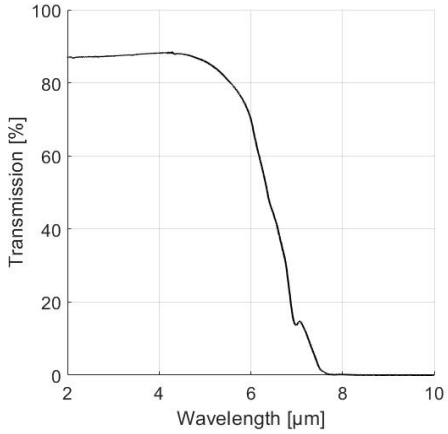


Fig. 10 – Transmission spectrum of sapphire

Regarding the two light transmission of the two top layers, we will consider for the rest of the study that they have a negligible effect on apparent emissivity. In other words, the emission involved by the phosphor and the sapphire substrate will be very low compared to the lower opaque layers.
Going down to the n-GaN active region, Welna *et al.* [31] have studied the optical behavior of GaN in the infrared region. The semiconductor doping influences the optical properties of GaN, notably with a shift of the absorption band towards short wavelengths. Moreover, for a concentration of free electrons about $10^{-19}cm^{-3}$, it has been shown that the N-type GaN becomes opaque in the spectral band [2 – 10]µm. **Tab. 4** sums-up which are the emission layer for each spectral band.

	Spectral band (µm)		
Layer considered	$0.4 < \lambda < 0.8$	$0.8 < \lambda < 7$	$7 < \lambda < 12.5$
Phosphor converter	Transparent	Transparent	Semi-transparent
Sapphire substrate	Transparent	Transparent	Opaque
n-GaN active region	Opaque	Opaque	N.A.

Tab. 4 – Spectral bands and opacity region (emission layer in grey)

To complete the trends presented in **Tab. 4**, we have performed a number of characterization on our LED using an IRTF Vertex Bruker 70 spectrometer, enabling measurement from 0.9 to 20µm (as illustrated in **Fig. 11**). Note that the "tested stack-up" in the band [0.8 – 7]µm is transparent-transparent-opaque: by knowing the apparent emissivity of the n-GaN (which is opaque through transparent layers), the temperature measurement will be done. The classical indirect way to perform an emissivity measurement is to use an integrating sphere to catch the entire light scattered in the hemisphere.

$$\varepsilon_\lambda = 1 - R_\lambda \#\text{Eq. (6)}$$

Due to the small dimensions of the LED, this approach is not possible due to the minimum dimension required for the sample to be tested with the integrating sphere. The adopted solution is to take advantage of the very small roughness induce on such micro-electronic manufactured devices. Indeed, Ruffenach-Clur *et al.* [32] have focused on process parameters involved in the GaN MOCVD growth process. At the end of the process, the rms rugosity Rq of the GaN sample was found to be 177nm. Based on that value, we can compare the standard deviation of roughness σ ($\sigma \approx Rq$) to the wavelength in the bandwidth [2.5 – 5]µm: $0.035 < \sigma/\lambda < 0.071$. Since $\sigma/\lambda \ll 1$, the GaN sample is specular in the bandwidth [2.5 – 5]µm, i.e. the entire reflected radiation is gathered into a small solid angle. To sum-up, integrating sphere is not necessary. A goniometer in Snell-Descartes conditions is then enough. The reflectivity distribution has been measured for an angle of

incidence of 13° and an angle of reflection varying between 13° and 80°, as shown in **Fig. 11**. The spot diameter is set to 0.5mm.

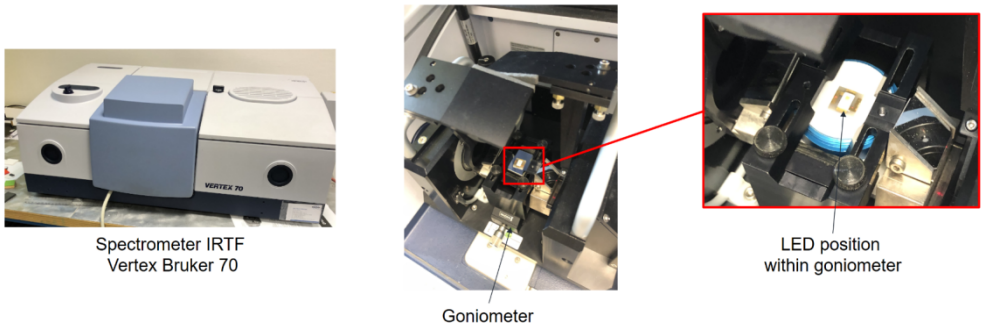


Fig. 11 – Experimental approach performed for characterizing LED emissivity

As shown in **Fig. 12**, the LED has a specular behavior in the spectral band [2.5µm – 5.5µm]. Indeed, 80% of the incident flux is reflected in a solid angle between 0° and 13°. Thus, the reflectivity characterization can be performed in Fresnel conditions. This confirms the assumption above.

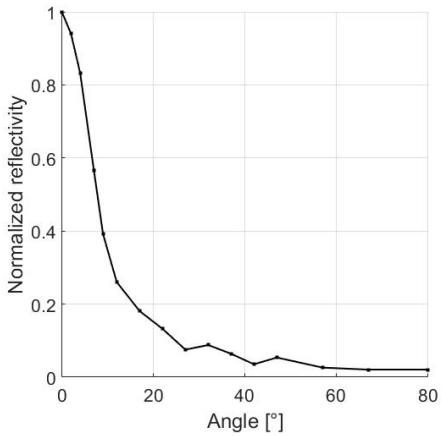


Fig. 12 – Normalized reflectivity of LED for a wavelength of 4µm

As shown in **Fig. 13**, in the spectral band [3 – 10]µm, it can be seen that the directional emissivity varies between 0.9 and 0.93, which means that the LED active region has the same behavior as a gray body.

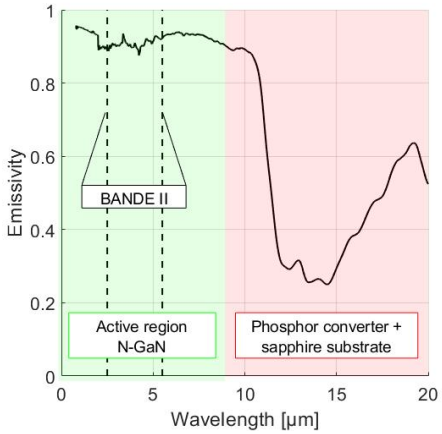


Fig. 13 – Directional emissivity of LED active region

For a wavelength greater than 6µm, the sapphire is opaque (*cf.* **Fig. 10**). The increase of emissivity in the bandwidth [6 – 8]µm is so due to the presence of sapphire. For a wavelength between 10µm and 13µm, a decrease of emissivity from 0.9 to 0.25 is noticeable. Then, a local maximum value of 0.65 is obtained at a wavelength of 18µm. Therefore, in the spectral band [10 – 20]µm, important variations of emissivity are highlighted. According to the previous information and characterizations, we knows that:

- The phosphor converter and sapphire layer are transparent between 2.5µm and 5.5µm.
- The LED active region is opaque between 2.5µm and 5.5µm and its emissivity is constant and equal to 0.9.

The LED active region has the same behavior than a grey body in the bandwidth [2.5 – 5]µm, with an emissivity of 0.9. Thus, to proceed to infrared thermography temperature measurement of the LED, an IR device operating in BII will be chosen.

3. Development of IR thermography test bench for LED temperature measurement

In this section, the development of an experimental in-lab set up used for measuring LED temperature is presented. Based on the previous results, it is possible to define the most adapted IR device. Then the calibration process and the uncertainties budget are going to be presented in order to define the total uncertainty of the measurement.

3.1. Experimental set-up and calibration

The choice of the IR device is influenced by several parameters such as the LED dimensions, temperature range and emissivity of the active region. On one hand, and as characterized in previous section, the active region is only accessible for wavelengths inferior to 7µm (*cf.* **Fig. 13**), where the sapphire substrate is transparent. On the other hand, the thermal range of interest ([20-140]°C) involves a maximum thermal emission above 7µm, so the wavelength needs to be as high as possible. Complying those two criteria, the choice of an InSb detector operating in BII ([2.5-5.5]µm) is optimal. Finally, the small dimensions of the LED determines the use of a macroscopic lens to avoid spatial subsampling errors. The final experimental set-up is then composed of a 14 bits FLIR SC7000 IR camera, Stirling cooled and equipped with a macro lens G1 Orion, which focal is 300mm. The value of the corresponding ΔX (projection of the pixel in the object plane) is about 30µm, which leads to a pixels number in the smallest dimensions of the phosphor converter of 46, sufficient for a good description of the LED thermal behavior. The characteristics of the final set-up are regrouped in **Tab. 5**.

Camera FLIR SC7000		**Macro lens G1 Orion**	
Detector type	InSb	Magnification	$1 \pm 5\%$
Spectral band	[2.5 – 5]µm	F number	$3 \pm 10\%$
Temperature range	5°C – 1500°C	Transmission	> 70%
Pixel resolution	320×256	Focal length – Field of View	300mm – 9.60×7.68mm
Pixel pitch	30µm	Working distance	300 ± 0.15mm

Tab. 5 – Technical characteristics of the experimental set-up

As illustrated on **Fig. 14**, the LED is mounted on its cooling system. The heat flux induced by the functioning of the LED is transfer to the cooling system using heat pipes. Then, the heat flux reaches a heatsink, on which a fan is blowing air, to ensure the cooling of the entire system. Finally, an

infrared camera FLIR SC7000 equipped with a macro lens G1 Orion is positioned in front of the LED to carry out its temperature measurement.

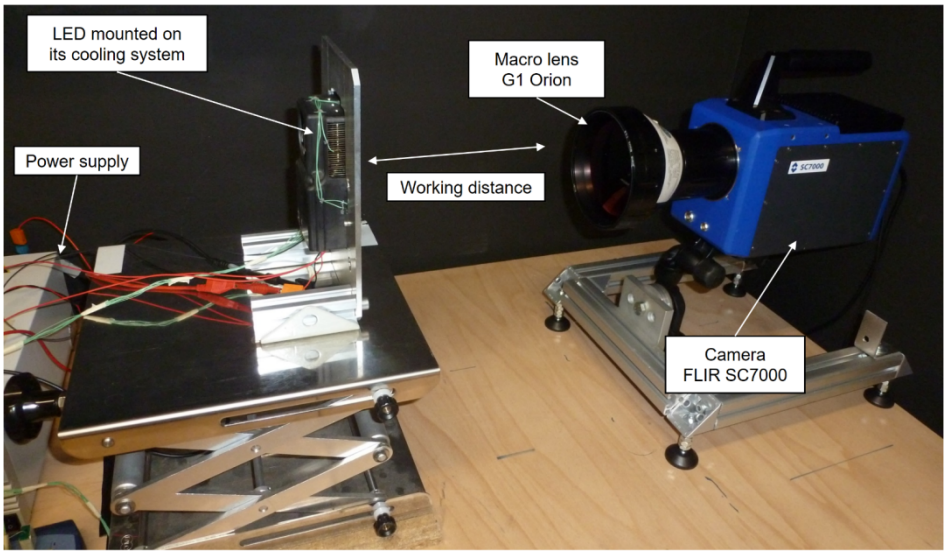


Fig. 14 – Experimental set-up: camera FLIR SC7000, macro lens G1 Orion and LED

As a new configuration, this set-up needs to be calibrated, placing a LANDCAL550P blackbody in front of the sensor and adjusting its temperature from 40 to 140°C, with a step of 20°C. A 9mm diaphragm is used to avoid the "size of source effect" (SSE) [33]. With that diaphragm, the blackbody radiation occupies around 4/5 of image. The integration time has been set at 75µs to ensure maximum digital levels for a blackbody temperature of 140°C. The aperture of the blackbody through the diaphragm (see **Fig. 15**-a) and the calibration curve obtained in the ROI 2 (see **Fig. 15**-b) is presented, associated with the interpolation error explained in next part.

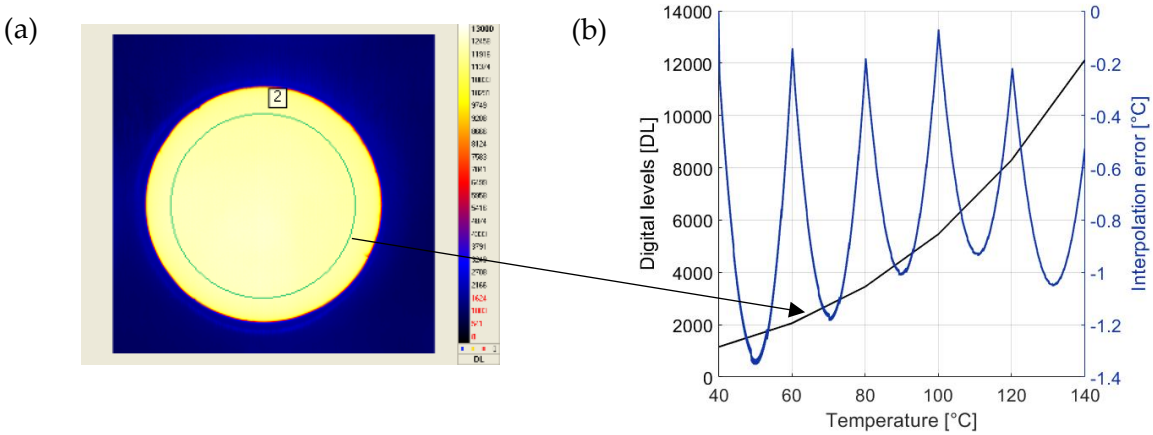


Fig. 15 – Aperture of the blackbody through the diaphragm Calibration curve of the IR camera SC7000 and associated interpolation error

The radiometric model used in the commercial Altair software furnished with the IR camera is a simple linear interpolation model. This latter is then perfectly accurate at the temperature used for

the calibration, but induces higher errors between each of these points. The evaluation of this error is presented in next part.

3.2. Uncertainty budget

The IR thermography purpose is to validate the thermal simulation model of high luminance LED. Moreover, as this model is planned to be used on industrial cases, its numerical cost (i.e. computing time, number of processors, etc.) must be minimized. The approach adopted here is then to construct a validation range instead of a singleton criterion, where the code results is included in the experimental error bars. This part is then dedicated to uncertainty budget of the IR temperature measurement, used for the LED thermal simulation validation.

- **Uncertainty budget evaluation methodology**

The first step of the uncertainty budget is to identify the sources of errors. The major contributions are gathered in **Tab. 6**, with their evaluation method. Note that others sources of errors have been investigated (influence of environment reflection, size-of-source effect, temporal drift, NETD) but, in our experimental conditions, are negligible.

	1	2	3	4
Error source	Interpolation error	Spatial heterogeneity	Spatial resolution	Emissivity
Evaluation method	Comparison of the approached model with a physical model	Spatial standard deviation calculation	Camera signal versus slit width	Analytical error calculation with monochromatic assumption

Tab. 6 – Error sources identification

A simple uncertainty propagation law is used here, according to Eq. (7), where k is the coverage factor, equal to 2. The total uncertainty, for each temperature j, is then proportional to the square root of the sum of each square standard deviations of the i^{th} error source.

$$\Delta T = k\sigma_T = k\sqrt{\sum_{i=1}^{N}\sigma_{T_{i,j}}^2} \qquad with\ i = 1,...,4\ \ and\ \ j = 1,...11 \#\text{Eq. (7)}$$

Note that the final error is calculated in the range 40 to 140°C, with a step of 10°C. Supplementary points were added to compare to the calibration data in order to demonstrate the effect of interpolation error, which is negligible for calibration points. Next points are dedicated to the evaluation of each standard deviation $\sigma_{T_{i,j}}$.

- **Errors induced by the radiometric model**

As seen above, the interpolation model is linear, and causes large errors between each calibration points. The evaluation of the error induced by such an approximation is performed by the comparison of this linear model with a physical model, which describes accurately the digital levels versus the temperature of the blackbody.

The reference model chosen is based on Wien's approximation as in [34], since the IR device operates in the spectral band [2.5 – 5]µm. This approximation is valid for the condition λT<2898µmK, respected for the maximum wavelength and temperature (for T=140°C and λ=5µm, λT=2065µmK). A two parameters model can then be used:

$$DL = A\exp\left(\frac{B}{T}\right) \#\text{Eq. (8)}$$

Fitting this model to experimental points by linear regression of the digital levels logarithm, the A and B constant are retrieved. The errors induced by such a model at the calibration temperatures do not exceed 0.34%. It can be considered as a reference model.
The difference between the reference and the linear model is displayed in **Fig. 15**-b. The interpolation error tends to zero at the calibration points and is maximum between two calibration points. It induces a maximum under-estimation of 1.4°C at 50°C (2.8%). The corresponding standard deviations are obtained considering a normal distribution of the error, inducing a coverage factor of 3 ($\sigma_{T_{1,j}} = \Delta T_{1,j}/3$). Numerical values are displayed in **Tab. 7** and show that the interpolation error globally decreases with temperature.

- **Spatial heterogeneity**

Thermal calibration is based on the blackbody radiation reference, supposed to show homogeneous, stable and isotropic radiation. Classical calibration method consists in calculating the signal spatial average inside a ROI for each temperature. Then, during the measurement, a unique set of calibration parameters are used for every pixels and the inversion of the model is performed. The spatial heterogeneity recorded (due to the blackbody or lens optical imperfections) is then a source of errors since it can bias the spatial average used for the calibration. In this study, this source of errors has been simply evaluated by measuring the thermal standard deviation in the blackbody aperture. The maximum value of this quantity $\sigma_{T_{i,2}}$ is around 0.7°C at 140°C (see **Tab. 7**) and slightly depend on the temperature.

- **Spatial resolution**

The small dimensions of the high luminance LED (3mm in with) may cause temperature errors due to spatial sub-sampling, even with the use of a G1 macro lens. To evaluate the impact of spatial resolution, several slits have been positioned between the reference source and the detector, as shown in **Fig. 16**. N slits widths are available in the laboratory: 0.69, 0.73, 1.16, 2.25 and 4.60mm.

(a) (b)

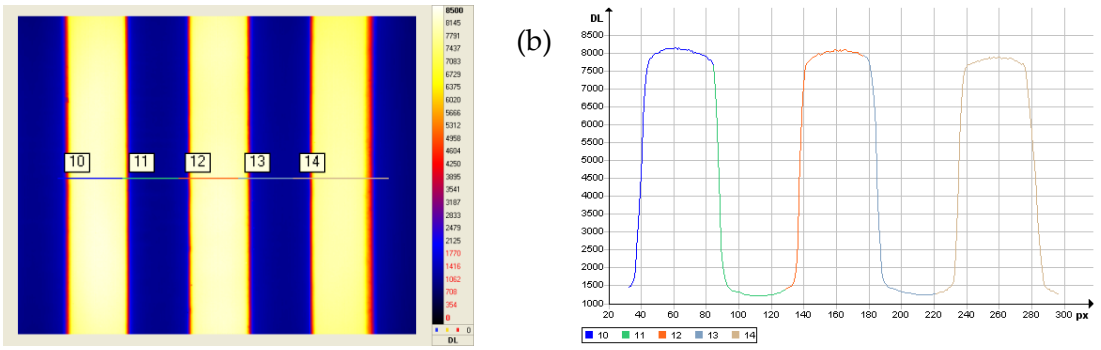


Fig. 16 – Infrared image of 2.25mm slit and selected tools (a), digital levels profiles (b)

For this evaluation, a temperature of 120°C has been considered to ensure sufficient signal for an integration time of 75µs. The reference signal is chosen at maximum slit width (4.6mm), as it should not be affected by spatial sub-sampling. The digital levels error induced by spatial sub-sampling for the k^{th} slit is then the difference between the intensity at the k^{th} slit width and the one at the maximum width slit ($k = N$):

$$\Delta DL_{i=3,j=10,\boldsymbol{k}} = DL_{i=3,j=10,\boldsymbol{k}} - DL_{i=3,j=10,\boldsymbol{k}=\boldsymbol{N}} \#\text{Eq. (9)}$$

This quantity is displayed in **Fig. 17** for the temperature of 120°C, which corresponds to a relative error on digital levels of around 4% for the minimum slit width. It is reduced to 0.74% for our LED dimensions (3mm). This value is then considered for the rest of study.

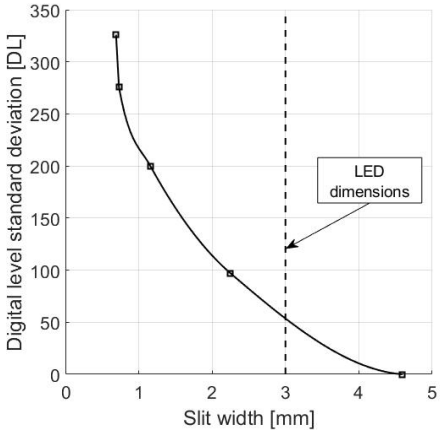


Fig. 17 – Deviation to the reference value as a function of the slits width

To retrieve the errors induced at other temperatures, the relative error previously calculated is supposed to remain constant, whatever the emitted flux:

$$\frac{\Delta DL_{i=3,j=10}}{DL_{i=3,j=10}} = \frac{\Delta DL_{i=3,j}}{DL_{i=3,j}} = 0.0074 \#\text{Eq. (10)}$$

The absolute digital levels error can then be calculated for each temperature. The standard deviation for each digital levels is then obtained inferring that the error distribution law is normal ($\Delta DL_{i=3,j} = 3 * \sigma_{DLi=3,j}$). Finally, the standard deviation on temperature is obtained using finite increments approximation:

$$\sigma_{Ti=3,j} \approx T\left(DL_{i=3,j} + \sigma_{DLi=3,j}\right) - T\left(DL_{i=3,j}\right) \#\text{Eq. (11)}$$

The numerical values are gathered in **Tab. 7**, and this standard deviation increases with temperature until it reaches the value of 0.47°C at 140°C.

- **Effect of emissivity**

An error on the emissivity induces an error on the measured temperature. The computation of the Planck's law derivative allows to estimate such an error, and applying a coverage factor of 3 enables to compute the standard deviation, according to Eq. (12)

$$\frac{\Delta T}{T} = \left| \frac{\exp\left(-\frac{C_2}{\lambda T}\right) - 1}{\frac{C_2}{\lambda T}} \right| \frac{\Delta\varepsilon}{\varepsilon} = k\frac{\Delta\varepsilon}{\varepsilon} \quad and \quad \Delta T_{i=4,j} = 3 * \sigma_{T_i=4,j} \#\text{Eq. (12)}$$

To maximize the error, a 5µm wavelength is considered. In addition, 10% relative error on emissivity is considered regarding the assumptions (transparency and opacity of the sub-layers) mentioned in the first section. The values obtained are regrouped in **Tab. 7**, and this standard deviation increases with temperature. The maximum reaches 0.39°C for 140°C.

- **Total uncertainty calculation**

The total uncertainty is included in **Tab. 7** and shows the same oscillations than the interpolation errors. Its value is maximum between each calibration points and is equal to 1.67°C at 140°C. A global increase in the total uncertainty is noticed, mainly linked with the emissivity effect. These values will be used in next section to validation the high luminance LED thermal model. In **Tab. 7**,

results obtained for temperature of 50°C and 110°C are highlighted, as they will be used in the following section.

T [°C]	40	50	60	70	80	90	100	110	120	130	140
Radiometric model	→0	0.67	→0	0.58	→0	0.33	→0	0.31	→0	0.34	→0
Spatial heterogeneity	0.46	0.48	0.42	0.48	0.42	0.48	0.43	0.48	0.47	0.48	0.68
Spatial sampling	0.20	0.25	0.22	0.28	0.26	0.32	0.29	0.36	0.32	0.40	0.47
Emissivity	0.09	0.11	0.14	0.16	0.19	0.22	0.25	0.29	0.32	0.36	0.39
Total error [°C]	**0.52**	**1.51**	**0.49**	**1.34**	**0.56**	**0.98**	**0.66**	**1.08**	**0.85**	**1.27**	**1.67**

Tab. 7 – Temperature standard deviations for each source of uncertainty and calculation of the total uncertainty

4. Simulation model and validation

In this section, the heat transfer model of the high luminance LED will be presented. Then, LED temperature measurements involving IR thermography are compared to numerical results in order to achieve thermal model validation.

4.1. Simulation set up

The LED stack-up structure has been reproduced in a commercial FVM simulation software FloEFD™. The equations are solved using stationary assumption, since only the stabilized temperature of the component is required. A hexahedral mesh has been involved with specific refinement in low thickness layers in order to ensure the capture of physical phenomena. A mesh sensitivity has been performed in order to define the most adapted mesh that allows ensuring moderated calculation time while ensuring a good prediction of physical phenomenon. In section 2.4, the energy balance related to LED has been presented. The determination of the thermal power dissipated by the source requires to know the consumed electrical power and the emitted optical power. The electrical power is determined from the measurement of current intensity and forward voltage ($P_{elec} = U * I$) while the optical power is determined from the measured luminous flux and luminous efficiency (*cf.* section 2.3). The thermal power per chip (see **Tab. 1**) is applied similarly to a uniform boundary condition in the LED chip as a volume heat source.

4.2. Validation of the LED heat transfer model

Once the LED thermal simulation model has been developed, the thermal resistance is used to validate the modeled stack-up structure used in the numerical simulation. For that, a cut plane has been used in order to show temperature gradient occurring in the LED thickness (see **Fig. 18**).

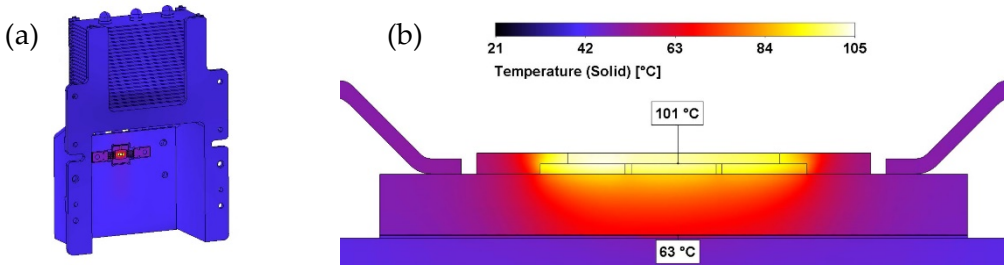


Fig. 18 - Thermal simulation of LED mounted on its cooling system for a current of 5A: view 3D (a) and cross-section (b)

The thermal resistance of the light source is determined as the ratio given by Eq. (13):

$$R_{th} = \frac{T_j - T_{case}}{P_{th}} \#\text{Eq. (13)}$$

where $T_j = 101°C$ is the junction temperature of the component, $T_{case} = 63°C$ is the substrate temperature and $P_{th} = 43.7W$ is the total dissipated power.

According to simulation results and after computation, the simulated thermal resistance of the component is equal to 0.87K/W, which is in good agreement with the value deducted from the cumulative structure function of the LED (*cf.* section 2.2): the deviation is lower than 3%. This allows validating the 3D model of the component. However, this latter can vary with power supply and possible ageing effects. Supplementary comparisons of simulation versus IR thermography is then necessary to validate completely the high luminance LED thermal model. **Fig. 19** proposes the visualization of the LED top view from experiment and simulation. At the active region location, thermography highlights a transversal temperature gradient occurring from left to right chip. It is also reproduced by simulation and is due to the non-uniform thermal power dissipated by the light source (*cf.* **Tab. 1**).

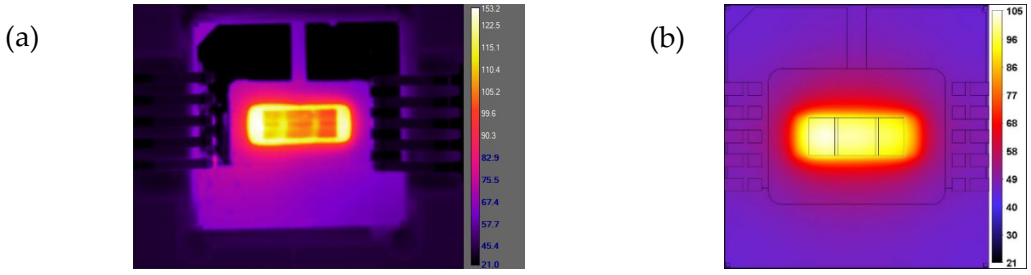


Fig. 19 – Top view of LED for a current intensity of 5A: IR thermography (a) and simulation (b)

Fig. 20 proposes the comparison of temperature profiles obtained for each configuration (i.e. I=2 and 5A). Herein, only the temperature of the active region is analyzed, represented by dashed lines on the following temperature profiles.

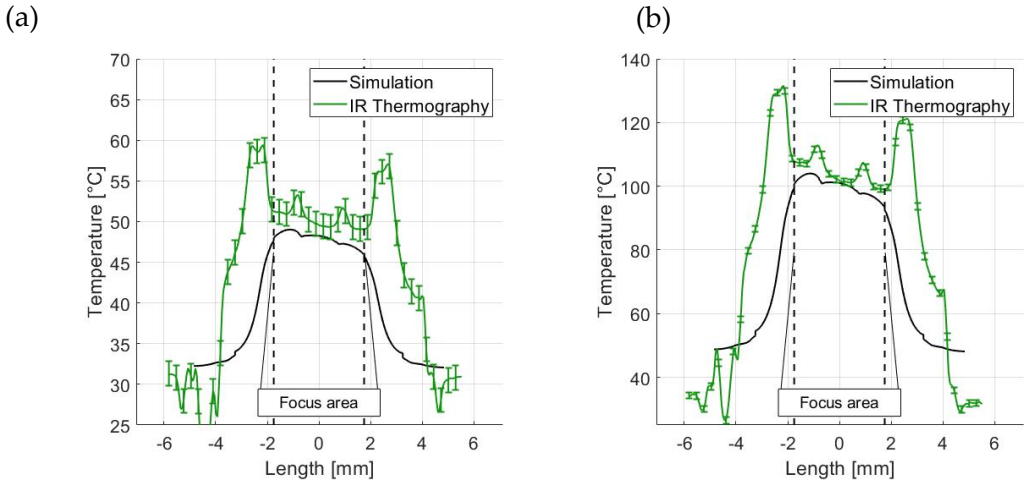


Fig. 20 – Temperature profiles obtained for a current intensity of 2A (a) and 5A (b)

For each configuration, temperature profiles are plotted (black line for simulation and green line for measurements), with error bars that correspond to the measurement uncertainty (according to **Tab. 7**). It can be seen that both simulation and IR thermography profiles agree well. The slope detected from IR thermography fits well the simulation, which means that the model is accurate.

Nevertheless, thermography highlights the presence of four peaks: the two interior peaks located at y ± 1mm are induced by the presence of silicone interstice deposited between each LED chip. The two other peaks at y ± 2mm are located at the active region / encapsulant interface. Each of them are induced by a change of emissivity: since the IR device is calibrated on the active region emissivity, only the temperature of this area is true. Regarding the temperature of the three LED chips, the results are in good agreement: the global deviation is lower than 5%, even on non-perfect component (as a reminder, the LED power distribution is asymmetric). Several ways can explain the remaining deviation. A sensitivity study based on both thermal resistance and power could take into account their measurement uncertainty. However, this can be fastidious since such a light source is still in development (the repeatability and reproducibility of the study may not be ensured). Last but not least, numerical error induced by the use of a commercial software could also explain a part of the deviation.

5. Conclusions

The main objective of this paper was to validate experimentally the thermal simulation model of a high luminance LED that dissipate a thermal power up to 40W. The simulation results were compared to IR thermography measurement. It can be noticed that:

- First, the full characterization of the component in terms of structural analysis, optical performances and thermal properties was performed for proceeding to the high luminance LED thermal model development.
- Then, and due to the small dimensions of the LED (and notably its active region), a well-designed IR spectrometry analysis was developed to measure the radiative properties of such a surface, since the emissivity is one of the fundamental parameters required for IR thermography measurement. Based on the LED active region opacity and emissivity value and according to the temperature level of LED in operating conditions, an IR camera operating in the spectral band [2.5µm – 5µm] has been defined as the most adapted device for proceeding to IR thermography measurement. The suggested method, which performed a non-contact temperature measurement, is based on IR thermography involving a macro lens G1. The calibration of the IR device has therefore been performed in order to measure quantitatively the LED temperature while evaluating the measurement error. The determination of such an error is based on a simple propagation of uncertainties.
- Finally, the 3D thermal simulation model of the high luminance LED was confronted to experiments in several operating conditions. The experimental set up developed for measuring the LED temperature leads to the validation of the high luminance LED thermal model.

To improve the thermal management of the LED, and so to decrease its temperature, one alternative may be to replace the current cooling system with a water-cooling system or a Pelletier module. This will decrease the LED temperature in order to preserve its performances.

One main perspective might be to reproduce similar experiments on other LED light sources (array LED, infrared LED, etc.). Moreover, it must be interesting to further investigate the propagation of uncertainties performed in this study and to proceed to emitting area emissivity characterization during a heating process, in order to evaluate more accurately the impact of temperature on

emissivity. Another interesting topic will be to investigate the thermal behavior of the component during an ageing process, and therefore understand its evolution in time.

References

[1] X. Morel,, S. Sommerschuh, H. El Idrissi et B. Reiss, «From discrete glare free to full HD lighting,» *Congrès Vision,* 2016.

[2] M. Courcier, B. Reiss et V. Sanchez, «New Front lighting possibilities through High Definition Digital Lighting,» *ISAL 2015,* 2015.

[3] C. Lasance et A. Poppe, Thermal management for LED application, New York: Springer, 2014.

[4] X. Huang, Y. Xu et W. Lin, «A new method of LED junction temperature modeling and measurement,» *2016 13th China International Forum on Solid State Lighting (SSL China),* pp. 48 - 51, 2016.

[5] T. Tetzlaff et U. Witkowski, «Estimation of LED junction temperature based on the forward voltage method for digital hardware implementation,» *2016 European Modelling Symposium (EMS),* 2016.

[6] D. Lee, H. Choi, S. Jeong, C. Jeon, D. Lee, J. Lim, C. Byon et J. Choi, «A study on the measurement and prediction of LED junction temperature,» *International Journal of Heat and Mass Transfer,* vol. 127, pp. 1243 - 1252, 2018.

[7] S. Labau, N. Picard, A. Gasse, S. Bernabe, P. Grosse et H. Ribot, «Chip on board packaging of light emitting diodes and thermal characterizations,» chez *Proc 59th Electronic Components and Technology Conf*, San Diego, USA, 2009.

[8] A. Corfa, A. Gasse, S. Bernabe et H. Ribot, «Analytical and FEM simulations of the thermal spreading effect in LED modules and IR thermography validation,» *2010 11th International Thermal, Mechanical & Multi-Physics Simulation, and Experiments in Microelectronics and Microsystems (EuroSimE),* 2010.

[9] J. Ling et A. Tay, «Measurement of LED junction temperature using thermoreflectance thermography,» *2014 15th International Conference on Electronic Packaging Technology,* pp. 1482 - 1485, 2014.

[10] D. Todorov, P. Mashkov, B. Gyoch et N. Mihaylov, «A study on thermal performance of LED signal heads using infrared thermography,» *Trans Motauto World,* vol. 2, n° %11, pp. 33-36, 2017.

[11] H. Jang, J. Lee, C. Byon et B. Lee, «Innovative analytic and experimental methods for thermal management of SMD-type LED chips,» *International Journal of Heat and Mass Transfer,* vol. 124, pp. 36-45, 2018.

[12] K. Yung, H. Liem et H. Choy, «Heat dissipation performance of a high-brightness LED package assembly using high-thermal conductivity filter,» *Applied Optics,* vol. 52, n° %132, 2013.

[13] I. Perera et N. Narendran, «Measuring the temperature of high-luminous exitance surfaces with infrared thermography in LED applications,» *15th International Conference on Solid State Lighting and LED-based Illumination Systems,* vol. 9954, p. 99540K, 2016.

[14] A. Aladov, A. Chernyakov et A. Zakgeim, «Infrared micro-thermography of high-power AlInGaN LEDs using high emissivity (black) in IR and transparent in the visible spectral region coating,» *Quantitative InfraRed Thermography Journal,* vol. 16, pp. 172 - 180, 2019.

[15] I. Perera, N. Narendran et Y. Liu, «Accurate measurement of LED lens surface temperature.,» *LED-based Illumination Systems,* vol. 8835, p. 883506, 2013.

[16] M. Ziegler, J. Tomm, T. Elsaesser, C. Monte, J. Hollandt, H. Kissel et J. Biesenbach, «Cavity-enhanced thermal emission from semiconductor lasers,» *Journal of Applied Physics,* vol. 103, n° %110, p. 104508, 2008.

[17] H. Zhang, R. Yang, Y. He, A. Foudazi, L. Cheng et G. Tian, «A review of microwave thermography nondestructive testing and evaluation,» *Sensors,* vol. 17, n° %15, p. 1123, 2017.

[18] W. Du, S. Addepalli et Y. Zhao, «The spatial resolution enhancement for a thermogram enabled by controlled subpixel movements,» *IEEE Transactions on Instrumentation and Measurement,* vol. 69, n° %16, pp. 3566-3575, 2019.

[19] A. Hermann, C. Rüssel et P. Pachler, «Ce3+ Doped yttrium aluminum and Lutetium aluminum garnet embedded in a soda-lime silica glass by a sintering technique,» *Optical Materials Express,* vol. 10, n° %15, pp. 2193-2200, 2015.

[20] L. Chen, W. Cheng, C. Tsai, Y. Huang, Y. Lin et Y. Cheng, «High performance glass phosphor for white-light emitting diodes via reduction of Si-Ce3+:YAG inter-diffusion,» *Optical Material Express,* vol. 4, n° %111, pp. 121-128, 2014.

[21] J. Wierer, D. Steigerwald, M. Krames, J. O'shea, M. Ludowise, G. Christenson, Y. Shen, C. Lowery, P. Martin, S. Subramanya, W. Götz, N. Gardner, R. Kern et S. Stockman, «High-power AlGaInN flip-chip light-emitting diodes,» *Applied Physics Letter,* vol. 78, n° %122, pp. 3379-3381, 2001.

[22] E. Deng, W. Chen, P. Heimler et J. Lutz, «Temperature Influence on the Accuracy of the Transient Dual Interface Method for the Junction-to-Case Thermal Resistance Measurement,» *IEEE Transactions on Power Electronics,* vol. 36, n° %17, pp. 7451-7460, 2020.

[23] D. Liu, H. Yang et P. Yang, «Experimental and numerical approach on junction temperature of high-power LED,» *Microelectronics Reliability,* vol. 54, n° %15, pp. 926 - 931, 2014.

[24] A. Alexeev, G. Marting et V. Hildenbrand, «Structure function analysis and thermal compact model development of a mid-power LED,» *33rd Thermal Measurement, Modeling & Management Symposium (SEMI-THERM),* pp. 283-289, 2017.

[25] H. Keitz, Light calculations and measurements: an introduction to the system of quantities and units in light-technology and to photometry, 1971: Macmillan International Higher Education.

[26] Y. Tyukhova et C. Waters, «An assessment of high dynamic range luminance measurements with LED lighting,» *Leukos,* vol. 10, n° %12, pp. 87-99, 2014.

[27] K. Sagawa et Y. Takahashi, «Spectral luminous efficacy as a function of age,» *JOSA A,* vol. 18, n° %111, pp. 2659 - 2667, 2001.

[28] F. Lacourarie, «Caractérisation thermique et lumineuse de diodes électroluminescentes en charge par méthodes locales non intrusives: influence du luminophore (in French),» Ecole nationale des Mines d'Albi-Carmaux, 2015.

[29] A. Khalifa, «Natural convective heat transfer coefficient-a review: I. Isolated vertical and horizontal surfaces,» *Energy conversion and management,* vol. 42, n° %14, pp. 491-504, 2001.

[30] G. Xia, S. Zhou, J. Zhang et J. Xu, «Structural and optical properties of YAG:Ce3+ phosphors by sol-gel combustion method,» *Journal of Crystal Growth,* vol. 279, n° %13-4, pp. 357-362, 2005.

[31] M. Welna, R. Kudrawiec, M. Motyka, R. Kucharski, M. Zajac, M. Rudzinski, J. Misiewicz, R. Doradzinski et R. Dwilinski, «Transparency of GaN substrates in the mid-infrared spectral range.,» *Crystal Research and Technology,* vol. 47, n° %13, pp. 347-350, 2012.

[32] S. Ruffenach-Clur, M. Moret, O. Briot, N. Moreau, J. Calas et R. Aulombard, «Optimization of the GaN epilayer quality using in-situ reflectance measurements.,» *MRS Online Proceedings Library,* vol. 639, n° %11, pp. 381-386, 2000.

[33] H. Yoon, D. Allen et R. Saunders, «Methods to reduce the size-of-source effect in radiometers,» *Metrologia,* vol. 42, n° %12, p. 89, 2005.

[34] T. Sentenac et R. Gilblas, «Noise effect on the interpolation equation for near infrared thermography.,» *Metrologie,* vol. 50, n° %13, 2013.

Acknowledgement

The authors would like to acknowledge Valeo Lighting Systems for having supported this work.